PET/EVA/PP Ternary Blends: An Investigation of Extended Morphological Properties

Mohamad Mahdi Abolhasani, Ahmad Aref Azar, Shirin Shokoohi

Department of Polymer Engineering, Amirkabir University of Technology, Tehran, Iran

Received 14 April 2008; accepted 6 November 2008
DOI 10.1002/app.29500
Published online 9 February 2009 in Wiley InterScience (www.interscience.wiley.com).

ABSTRACT: In this study, the effects of different parameters on the morphological properties of ternary blends were investigated. Therefore two systems (PET/H-EVA/PP and PET/L-EVA/PP, H-EVA and L-EVA are high and low viscosity, respectively) were prepared by melt mixing process. In all of the blends, poly (ethylene terephthalate) (PET) as the major phase- with poly propylene (PP) and two grades of poly (ethyl-stat-vinylacetate) (EVA) with different viscosities and subsequently different interfacial interactions was blended. Theoretical models predicted positive spreading coefficient for two grades of EVA and lower free energy for the samples consisting of EVA and PP as the shell and the core phases respectively. With changing core shell ratio, droplet size of samples containing L-EVA and H-EVA increased and decreased, respectively. Subinclusion of shell into the core was observed in some blended samples. In systems containing H-EVA, by thickening the shell phase; multi core morphology was observed which would be related to the coalescence phenomenon inter the droplets. © 2009 Wiley Periodicals, Inc. J Appl Polym Sci 112: 1716–1728, 2009

Key words: blend; morphology; core-shell polymers

INTRODUCTION

Polymer Blending is one of the most important techniques of producing new materials with desirable characteristics such as considerable mechanical properties, low economical cost considerations compared to the other new methods for new polymers synthesis.[1–3] Most of the articles about polymeric blends are related to the binary polymer blend systems in which the minor phase has been dispersed into the major phase. Since mechanical properties of polymer blends are intensively influenced by their morphology, control of morphology has become a important matter for polymer engineers consideration.

Effects of blending history, composition, interfacial tension and viscosity ratio of polymers on the morphology of blends have been investigated.[4–8] Recently, some researches have been focused on ternary blend systems.[9–23] The effect of mentioned factors on the morphology of ternary blends has also been investigated.[9–23] Blend morphology prediction has been mostly done using different equations. Hobbes et al.[17] have rewritten the Harkin's[24] equation for a ternary system where A is the continuous phase and B, C are the dispersed phases. For B-phase on C-phase:

$$\lambda_{BC} = \gamma_{AC} - \gamma_{BC} - \gamma_{AB} \tag{1}$$

where γ_{AC}, γ_{BC}, γ_{AB} are interfacial tensions between phases. If λ_{BC} is positive, then B-phase will encapsulate the C-phase and, so, for the C-phase on the B phase, the related equation is:

$$\lambda_{CB} = \gamma_{AB} - \gamma_{BC} - \gamma_{AC} \tag{2}$$

Positive values of λ_{CB} implicate encapsulating of the B-phase by the C-phase. Negative values of λ_{BC} and λ_{CB} lead to dispersion of individual B and C phases in the A matrix. Guo et al.[12,13] showed that the morphology obtained in multi phase systems, is determined not only by interfacial tensions, but also by the interfacial free energy which includes the interfacial area besides the interfacial tension. The free energy of mixing independent of the morphology type could be written as:

$$G = \sum_i n_i \mu_i + \sum_{i \neq j} A_{ij} \gamma_{ij} \tag{3}$$

where μ_i is the chemical potential parameter, n_i is the number of i the moles and A_{ij}, γ_{ij} are the interfacial area and the interfacial tension between components i and j respectively. The first term in the Eq. (3) is equal for all types of morphologies but the second term will be different. Guo et al.[12,13] proposed a substitution for the second term of this equation as:

$$\left(\sum A_i \gamma_{ij}\right)_{B+C} = (4\pi)^{1/3}[n_B^{1/3} X^{2/3} \gamma_{AB} + n_c^{1/3} \gamma_{AC}] \times (3V_C)^{2/3} \tag{4}$$

Correspondence to: A. A. Azar (arefazar@aut.ac.ir).

$$\left(\sum A_i\gamma_{ij}\right)_{B/C} = (4\pi)^{1/3}[n_B^{1/3}(1+x)^{2/3}\gamma_{AB} + n_C^{1/3}\gamma_{BC}] \times (3V_C)^{2/3} \quad (5)$$

$$\left(\sum A_i\gamma_j\right)_{C/B} = (4\pi)^{1/3}[n_B^{1/3}x^{2/3}\gamma_{BC} + n_C^{1/3}(1+x)^{2/3}\gamma_{AC}] \times (3V_C)^{2/3} \quad (6)$$

where A_i is the interfacial area of each phase in the system, $x = V_B/V_C$, $V_i$is the volume of each phase, and n_B and n_C are the numbers of particles in the B and C phases in the system, respectively. They assumed that $n_B = n_C$ and calculated the interfacial energy for each phase structure.

Hemmati et al.[21] used Guo's equation for core-shell and dispersed morphologies in the form of following equations and renamed it as "Relative Interfacial Energy (RIE)":

$$(\mathrm{RIE})_{B+C} = \left(\sum A_i\gamma_j\right)_{B+C}/K = x^{2/3}\gamma_{AB} + \gamma_{AC} \quad (7)$$

$$(\mathrm{RIE})_{B/C} = \left(\sum A_i\gamma_{ij}\right)_{B/C}/K = (1+x)\gamma_{AB} + \gamma_{BC} \quad (8)$$

$$(\mathrm{RIE})_{C/B} = \left(\sum A_i\gamma_{ij}\right)_{C/B}/K = [x^{2/3}\gamma_{BC} + (1+x)^{2/3}\gamma_{AC}] \quad (9)$$

where $x = V_B/V_C$, γ_{ij} is the interfacial tension between two phases, $K = (4\pi)^{1/3}\ n_C^{1/3}\ (3V_C)^{2/3}$ and $(\mathrm{RIE})_{B+C}$ denotes the relative interfacial energy for the separately dispersed morphology of the two minor components, $(\mathrm{RIE})_{B/C}$ for the morphology in which the B-phase encapsulates C, and $(\mathrm{RIE})_{C/B}$ for the morphology in which the C-phase encapsulates B. The most stable morphology has the minimum value of $\Sigma_{i+j}A_{ij}\gamma_{ij}$ which results in minimum Gibbs' free energy value consequently.

Both the minimal free energy surface and spreading coefficient has been employed by many researchers to predict the morphology of ternary blends.[12,14,17,20–22] Vanoene et al.[25] showed that in the dynamic flow conditions, the elasticity difference between the phases of binary blends can influence the interfacial tension value so that the interfacial tension would be completely different from that of the static flow conditions. When the matrix is more elastic than the disperse phase, dynamic interfacial tension is less than the static interfacial tension. According to Vanoene's results and his proposed substitution in Guo's equations, Reignier et al.[16] obtained the following equations:

$$\left(\sum A_i\gamma_{ij}\right)_{B/C} = 4\pi R_e^2\left[\gamma_{BA} + \frac{R_e}{6}\left(N_{1,B} - N_{1,A}\right)\right] + 4\pi R_i^2\left[\gamma_{CB} + \frac{R_i}{6}\left(N_{1,c} - N_{1,B}\right)\right] \quad (10)$$

$$\left(\sum A_i\gamma_{ij}\right)_{C/B} = 4\pi R_e^2\left[\gamma_{CA} + \frac{R_e}{6}\left(N_{1,C} - N_{1,A}\right)\right] + 4\pi R_i^2\left[\gamma_{BC} + \frac{R_e}{6}\left(N_{1,B} - N_{1,C}\right)\right] \quad (11)$$

$$\left(\sum A_i\gamma_{ij}\right)_{B+C} = 4\pi R_i^2\left[\gamma_{BA} + \frac{R_i}{6}\left(N_{1,B} - N_{1,A}\right)\right] + 4\pi R_i^2\left[\gamma_{CA} + \frac{R_i}{6}\left(N_{1,C} - N_{1,A}\right)\right] \quad (12)$$

where N_1 is the first normal stress difference for A, B and C phases, R_i and R_e are the internal and external radius of core-shell droplets and γ_{ij} is the interfacial tension between components ***i*** and *j*.

Reignier and Favis[15] predicted the encapsulations of high molecular weight PS by PMMA in HDPE/PS/PMMA ternary blend systems by the employment of this model while other models couldn't result as well.

The rheological properties of participating polymers can affect the morphology of ternary systems.[18–23] In particular, the ratio of elasticity[23] and viscosity[18–22] of the two minor phases and their effect on the morphology were investigated.

However, some authors have observed the component with the less viscosity; encapsulate the component with higher viscosity.[18,26] Yet some others observed the contrary[19] and also there are some reports claiming ineffectiveness of the ratio of viscosities on the morphology type.[15,21–22] Reignier et al.[15] showed that to investigate the effect of the viscosity ratio on the morphology, the viscosity ratio should be calculated in a constant shear stress rather than a constant shear rate; because the continuity of the shear stress is more in the droplet-matrix interface compared to the shear rate. PS/SBR/PE polymer blends containing components with different viscosity ratios were also studied by Luzinov et al.[27] They assumed "core to shell viscosity" as a measure of the core diameter and "shell to matrix viscosity" as a measure of dispersed phase diameter. Hemmati et al.[21] suggested a relationship between the steady state torque and viscosity; they also showed the average torque ratio of two minor phases to matrix as a criterion of core-shell droplet diameter. In constant compositions of the dispersed phase, Reignier and

TABLE I
Material Characteristics

Polymer	Melt index[a] (ASTM) (g/10 min)	Density (g/cm^3) at 20°C	M_n	M_w	η*(Pa.s) at 260°C $\dot{\gamma}$= cte[b]	η*(Pa.s) at 260°C τ = cte[c]	N_1 (Pa) × 10^{-3} at 260°C $\dot{\gamma}$= cte[b]	N_1 (Pa) × 10^{-3} at 260°C τ = cte[c]	VA Contents HPC WE%	Producer
PET	–	1.3	1.8×10^{4a}	3.2×10^{4a}	64	64	7.99	7.99	—	PARS, Iran petrochemical
PP	1.8[d]	0.9	7.9×10^{4a}	4.1×10^{5a}	90	105	12.45	8.18	—	HP500H, Iran petrochemical
H-EVA	1.7[e]	0.939	6.1×10^{4f}	2.4×10^{5f}	301	876	104.61	13.20	18	V3430, Hyundai SEETEC
L-EVA	400[e]	0.95	1.5×10^{4f}	3.4×10^{4f}	10	10	2.22	114.81	28	VA910, Hyundai SEETEC

[a] Obtained from suppliers.
[b] Average shear rate during blending: $\dot{\gamma}$= 150 s^{-1}.
[c] Average shear stress during blending: τ = 9630 Pa.
[d] ASTM D1238/L.
[e] ASTM D1238.
[f] Measured by GPC.
* Characteristics of the material used.

Favis showed that with increasing the amount of the component with higher viscosity, the droplet size also increases. They also attributed this behavior to the increment of the droplet to matrix viscosity ratio.[14] On the contrary, Valer et al.[22] claimed that increasing the component of higher viscosity decreased the droplet size; while the shell thickness was constant and the extra PS became individual particle in the matrix. They claimed that this behavior is because of decrement of the interfacial tension.

In this work the morphology of PET/EVA/PP blends with different compositions was investigated. Results were compared to the spreading coefficient, relative interfacial energy and dynamic interfacial energy model. Changes in the droplet size with the core/shell composition ratio variations, the effect of viscosity fluctuation on the core-shell size and its formation state, and influencing parameters on the internal structure of droplets were also investigated.

EXPERIMENTAL

Materials

The Poly (ethylene terephthalate) (PET), intrinsic viscosity of 0.64 dL/g, two types of poly (ethylene-stat-vinyl acetate) (EVA) (L-EVA and H-EVA nomenclature as the low and high viscosity) and poly propylene (PP) used in this study. Characteristics of the homopolymers are summarized in Table I.

Mixing process

Melt mixing was carried out in a 60 mL Brabender internal mixer, at 260°C and rotor speed of 50 rpm. The EVA was added to the molten PET/PP mixture after 4 min from the mixing start. The overall mixing time was set to be 7 min and the outgoing blend was directly quenched in the cold water to fix the morphology.

The average shear rate of the mixer was estimated via Bousmina's equation[28] to be about 150 s^{-1}. The matrix shear stress in this shear rate is about 9630 Pa. Table II shows details of all prepared blends of PET/EVA/PP(X/Y/Z) which X, Y and Z indicate volume fraction of PET, EVA and PP respectively. Samples 1–7 (Table II) have the same disperse phase composition but different EVA/PP ratio, in samples 5, 6, 8, and 9 have the equal amounts of EVA and PP, but the disperse phase content is varied and samples 10–17 are the reference binary blends.

TABLE II
All Samples were Prepared

Sample[a]	Major phase	Minor phase (1)	Minor phase (2)
1	PET (70)	H-EVA (5)	PP (25)
2	PET (70)	L-EVA (5)	PP (25)
3	PET (70)	H-EVA (10)	PP (20)
4	PET (70)	L-EVA (10)	PP (20)
5	PET (70)	H-EVA (15)	PP (15)
6	PET (70)	L-EVA (15)	PP (15)
7	PET (70)	H-EVA (23)	PP (7)
8	PET (80)	L-EVA (10)	PP (10)
9	PET (90)	L-EVA (5)	PP (5)
10	PET (70)	–	PP (30)
11	PET (80)	–	PP (20)
12	PET (90)	–	PP (10)
13	PET (80)	L-EVA (20)	–
14	PET (90)	L-EVA (10)	–
15	PET (70)	H-EVA (30)	–
16	PET (80)	H-EVA (20)	–
17	PET (90)	H-EVA (10)	–

[a] Numbers in parentheses represents the volume phase content.

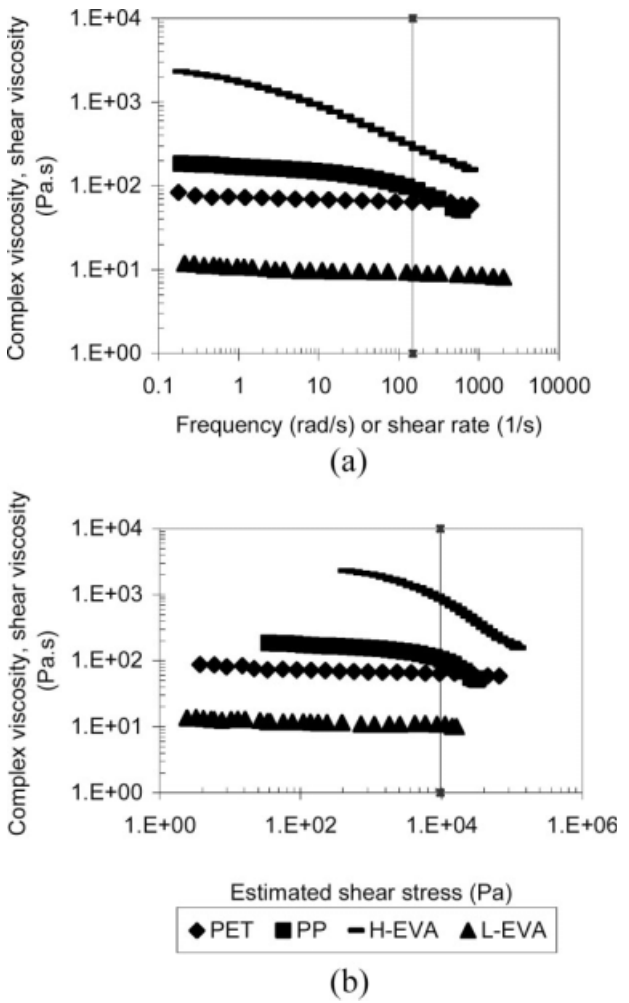

Figure 1 (a) Complex viscosity and shear viscosity as functions of frequency and shear rate, respectively. (b) Complex viscosity and shear viscosity as functions of estimated shear stress.

Rheological analysis

Rheological characterization of the homopolymers was carried out using a Physica Anton Paar (MCR300) Rheometer. Experiments were performed in a parallel-plate geometry with a gap of 1 mm space under nitrogen atmosphere at the temperature of 260°C. Strain sweep tests were performed to determine the linear viscoelasticity region. The rheological properties of the polymers used here, are shown in Figure 1 and Table I.

Morphological analysis

The specimens used for the morphological analysis were cryogenically broken in the liquid nitrogen and then the fracture surface was put into toluene for 2 h for blends containing L-EVA and 3 h for blends containing H-EVA at 50°C under string to dissolve the EVA. The etched fracture surfaces were coated with gold and observation was done with a Jeol JSM 840 scanning electron microscope operating at a voltage of 20 Kv. The average particle size of about 250 particles for each blend was calculated using in-house software.

RESULTS AND DISCUSSION

Interfacial tension

Surface tension values of PET, PP and two types of EVA at 260°C were calculated on the basis of the data reported for surface tensions (γ), at 200°C, variation rate of surface tensions with temperature ($-d\gamma/dt$), and polarities ($x_p = \gamma_p/\gamma$).[29] The surface tension γ, the dispersive contribution of $\gamma(\gamma_d)$ and polar contribution of $\gamma(\gamma_p)$ for all of the polymers used here, are listed in Table III. The interfacial tension between the polymers can be calculated from the well-known harmonic mean equation as below:

$$\gamma_{12} = \gamma_1 + \gamma_2 - \frac{4\gamma_{1d}\gamma_{2d}}{\gamma_{1d} + \gamma_{2d}} - \frac{4\gamma_{1p}\gamma_{2p}}{\gamma_{1p} + \gamma_{2p}} \qquad (13)$$

The interfacial tensions calculated from the surface tension data at 260°C are listed in Table IV.

Rheological characterization

Figure 1(a,b) show the viscosity of PET, PP, H-EVA and L-EVA as a function of shear rate or frequency; and the viscosity of the polymers mentioned above, as a function of the estimated shear stress respectively. The shear stress was estimated by the product

TABLE III
Surface Tension of Polymers

Polymer	γ (200°C) mN/m	$-d\gamma/dT$ $(mN/m/K)$	Polarity (x^P)	γ (260°C) mN/m	γ_p (260°C) mN/m	γ_d (260°C) mN/m
PET	33.5	0.065	0.221	29.6	6.5	23.0
H-EVA	24.9	0.054	0.025	21.7	0.5	21.1
L-EVA	25.1	0.037	0.064	22.9	1.6	21.3
PP	19.8	0.056	0	16.5	0	16.5

TABLE IV
Estimated Interfacial Tension at 260°C

Interface	Interfacial tension at 260°C (mN/m)
PET/PP	7.65
PET/H-EVA	5.17
PET/L-EVA	3.088
PP/H-EVA	1.11
PP/L-EVA	2.22

of the angular frequency and the measured complex viscosity.

It can be observed in Figure 1(a) that for an average shear rate of 150 s^{-1} the range of viscosity is $\eta_{H-EVA} > \eta_{PP} > \eta_{PET} > \eta_{L-EVA}$. In Figure 1(b) the range of viscosity is the same for the shear stress corresponding to the matrix shear stress.

Using equation 14 and 15 the steady shear viscosity and first normal stress difference of pure polymers were calculated. The well-known Cox-Merz equation.[30]

$$\eta_S = \frac{G''}{\omega}\sqrt{1+\left(\frac{G'}{G''}\right)2} \text{ for } \omega = (\dot{\gamma}) \qquad (14)$$

relates the dynamic viscosity $|\eta^*(\omega)|$ obtained from rheological measurement to study shear viscosity. Then complex viscosity versus frequency can be considered as steady shear viscosity versus shear rate.

An empirical relation which relates the steady state normal stress coefficient to dynamic properties was found by laun[31]:

$$\psi_1(\dot{\gamma}) = 2\frac{G'}{\omega^2}\left[1+\left(\frac{G'}{G''}\right)^2\right]^{0.7} \text{ for } \omega = (\dot{\gamma}) \qquad (15)$$

It is verified that this relation works well for many polymers. Figure 2 presents the first normal stress difference as a function of shear rate and shear stress. Table I presents the viscosity of polymers and the first normal stresses at the applied shear rate and shear stress undergone by the matrix. The first normal stress difference in the average shear rate of 150 s^{-1} can be sorted as $N_{1H-EVA} > N_{1PP} > N_{1PET} > N_{1L-EVA}$ and for the matrix shear stress, $\tau = 9630$ Pa, the first normal stress is as $N_{1L-EVA} > N_{1H-EVA} > N_{1PP} > N_{1PET}$. The vertical line in Figures 1(a) and 2(a) represents the applied shear rate (150 s^{-1}), and the vertical line in Figures 1(b) and 2(b) represents the shear stress undergone by the matrix (9630 Pa.). As an important point of view, it should be noticed how the viscosity and elasticity ratio are estimated and which criteria is better for this estimation, constant shear rate or constant shear stress. Although in multi phase system, the velocity may be continuous at the interface of surface of a droplet under deformation but the local shear rate may be discontinuous. On the other hand it can be assumed that the interface only transmits the shearing stress between two fluids, so the local shear stress may be continuous. Therefore, it seems that the shear stress is a more suitable criterion for comparing viscosity and normal forces. Because of some uncertainties about the use of a constant shear rate or constant shear stress in the comparison of the rheological properties of multi phase systems, both of the variables will be examined in this work.

Predictions of models

To predict the phase morphology spreading coefficient, RIE and DIE models were calculated from equations 1–12. The calculated results of spreading coefficient, relative interfacial energy and dynamic

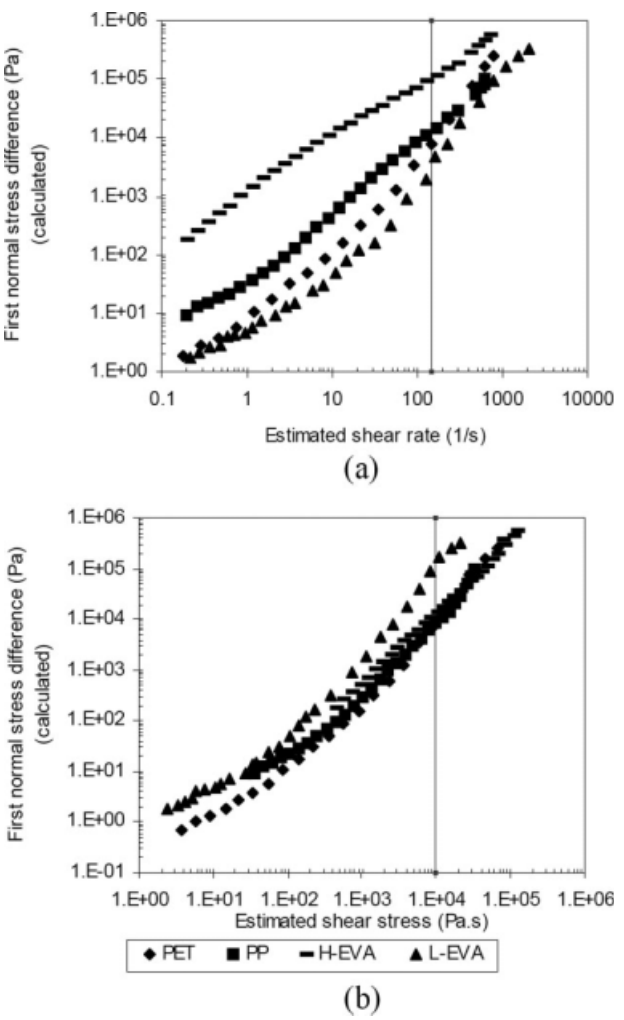

Figure 2 (a) First normal stress difference as a function of frequency and shear rate. (b) First normal stress difference as a function of estimated shear stress.

TABLE V
Morphology Predicted by Spreading Coefficient

Ternary polymer blend	$\lambda_{C/B}$[a]	$\lambda_{B/C}$[a]
PET/H-EVA/PP	−3.59	1.37
PET/L-EVA/PP	−6.78	2.34

[a] B phase is EVA and C phase is PP.

interfacial energy are shown in Table V to 7, respectively. Although the discussed models have been used by several researchers to predict the morphology of ternary blends, their ability of prediction with composition and operational condition changes, has not studied yet. In contrast to prediction of spreading coefficient model which are not sensitive to composition, predictions of RIE and DIE equation is sensitive to this parameter. Assessment of predictions of these models with operational conditions is not scope of present article.

To calculate DIE, following Reignier et al.[15] assumptions which hold that all the studied structures have the same number of particles of the dispersed phase and also negative values of the dynamic interfacial tension could be set equal to zero were applied. Some of their assumptions were not applicable in this research work; particularly the assumptions $R_e = 3\sqrt{2}R_i$ and $R_i = R_e$ for core-shell (B/C and C/B) and separated dispersion of both dispersed phase morphologies (B+C), respectively, (R_i and R_e are the internal and external radius of core-shell droplets). It was assumed that $V_{droplet} = 5\ \mu m^3$, instead $R_i = 1\mu m$ considered by Reignier, then R_i to R_e ratios was calculated in different composition, regarding reference volume. It was obvious that considering another reference volume doesn't change these calculations. Only when the ratio of core to shell equals to unity, the Reignier assumption, $R_i = 1\mu m$, can be used. See Figure 3 for better understanding. Valera et al.[22] showed that for B+C morphology when $\lambda_{AB} \approx \lambda_{AC}$ (happens while using L-EVA in this work) $R_i = R_e$, and when λ_{AB} is different from λ_{AC} (happens while using H-EVA in this work) the radius ratio of both separated disperse phase ($\frac{R_B}{R_C}$) could be obtained from the experimental values of R_B and R_C in the related binary blends (A/B and A/C blends). In the present work, for B+C morphology calculations were performed twice. First, R_B and R_C were obtained on the base of reference volume and B to C phase volume ratio. On the other way, these were calculated according to size of B and C phase in the respective binary blends. It is worth noting that the EVA phase is assumed to be situated at the interface and all the PP phase is only present as the core it means that no individual EVA and PP particle can be observed in the matrix phase.

Results of Table V indicate that for all ternary blends, λ_{CB} and λ_{BC} are negative and positive, respectively, which are in a good agreement with the resulted morphology. One can see from Table VI that the morphology in which the B-phase encapsulates the C-phase (B/C) has the lowest value of Relative Interfacial Energy for all the blends with different compositions and EVA contents. It is clear that RIE model predicts correctly with composition change. Some researchers report that some droplets of shell forming material enter the matrix with increasing the shell thickness.[22] The effect of composition on the prediction results of DIE and RIE models has been investigated to see if the increment of core to shell portion will change the model prediction to B+C type morphology; as it will be shown that it is not the case for this blend. The other model used to predict the morphology was Dynamic Interfacial Energy. Table VII shows that for the ternary blends with H-EVA, in a constant shear stress, the B/C morphology always has the minimum DIE values except for PET/H-EVA/PP(70/5/25) blend and in constant shear rate it predict different morphologies. It will be showed that in PET/H-EVA/PP(70/5/25) blends the shell dose not cover the core completely, therefore, the assumption used for the DIE equation are not accurate and it is obvious that the prediction of the model will not be correct. In the blends with L-EVA as the shell phase, L-EVA covers the core thoroughly; even with 5% (% vol.). This phenomenon can be related to lower molecular weight of L-EVA than H-EVA. For the blends with L-EVA as the shell, DIE predicted the encapsulation of

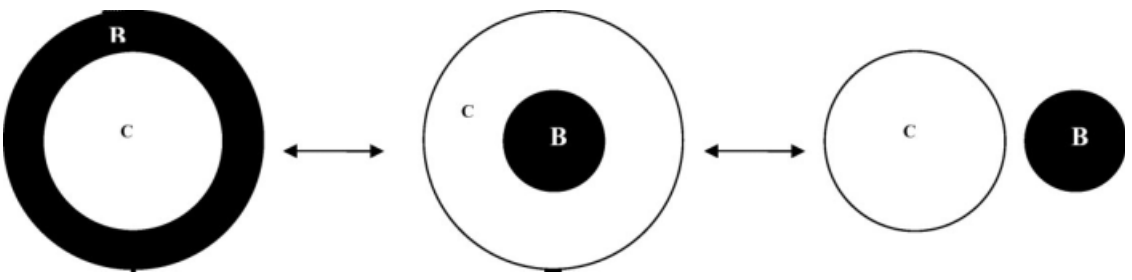

Figure 3 Schematic representation of calculation method of internal and external radiuses ($R_i$and R_e) of core-shell particles.

TABLE VI
Relative Interfacial Energies for (PET/EVA/PP) Ternary Blends at Different Compositions

Sample	$x = V_B/V_C$ [b]	RIE_{B+C} [b]	$RIE_{B/C}$ [b]	$RIE_{C/B}$ [b]
2	0.2	9.32	6.94	11.08
4	0.5	10.81	7.88	12.47
1	0.2	9.5	5.7	13.53
3	0.5	8.61	6.26	14.92
5	1	10.73	7.12	14.22
7	3.28	18.97	14.73	22.61

[a] See Table 2.
[b] B phase is EVA and C phase is PP.

PP by L-EVA (B/C) for constant shear rate. On the other hand, in constant shear stress DIE showed B+C morphology. Therefore it can be concluded that in high viscosity difference, the calculation of N_1 in average matrix stress (9630 Pa) is not suitable for DIE model. It seems that stress at the L-EVA/PP interface is not equal to average matrix stress. Finding an accurate method for estimation of dynamic interfacial tension is a challenging problem. Therefore, according to other works,[14] DIE model should not be regard as a comprehensive predictive model.

Morphology of the blends

Figures 4 and 5 show SEM micrographs of samples 1–7. At first glance to the SEM micrographs of etched ternary blends one may doubt to the formation of core–shell morphology. However, to discriminate between core–shell morphology and voiding phenomenon that occurs while sample is cooling, PET/H-EVA/PP(70/15/15) and PET/H-EVA(70/30) both without etching was compared.

As can be seen from Figure 6(a), for PET/H-EVA(70/30) some voiding has been occurred around the H-EVA droplets. This phenomenon is related to different change in specific volume versus temperature for PET and H-EVA. Formation of voiding was previously reported by Leclair et al.[32] for HDPE/PC blends. It is obvious that this voiding phenomenon is much smaller than possible void due to EVA removal by toluene.

To emphasize on formation of core–shell morphology micrograph of ternary blends of PET/H-EVA/PP (70/15/15) without etching is added [Fig. 6(b)]. Formation of core–shell morphology by comparing Figure 6(a,b) is obvious.

As can be seen in all of the blends, PP is encapsulated by EVA (L-EVA or H-EVA); this is in a good agreement with the spreading coefficient and relative interfacial energy predictions. The pictures correspond to the 30% of the disperse phase. In the case of PET/L-EVA/PP(70/15/15) ternary blends, a cocontinues phase morphology was observed [Fig. 5(c)]. With altering the L-EVA/PP ratio from 15/15 to 10/20, the cocontinues morphology changes to the core–shell morphology (Fig. 5) that could be attributed to the increase in the average droplet viscosity.

As can be seen, the fracture has happened at the cross section of droplets not at the interface, and this is an evidence of desirable mechanical properties.

TABLE VII
Values of the Dynamic Interfacial Energy for PET/EVA/PP ternary blends

EVA/PP		Dynamic interfacial energy (Nm/particle)					
		B=H-EVA, C=PP			B=L-EVA, C=PP		
		B + C	B/C	C/B	B + C	B/C	C/B
$\frac{5}{25}$	Shear stress constant	2.75×10^{-14} 1.22×10^{-13}[a]	8.59×10^{-14}	1.16×10^{-13}	6.81×10^{-14} 1.35×10^{-13}[a]	3.09×10^{-13}	1.71×10^{-13}
	Shear rate constant	1.75×10^{-13} 1.86×10^{-13}[a]	3.14×10^{-13}	1.71×10^{-13}	1.14×10^{-13} 1.23×10^{-13}[a]	7.70×10^{-14}	1.25×10^{-13}
$\frac{10}{20}$	Shear stress constant	1.22×10^{-13} 1.20×10^{-13}[a]	8.59×10^{-14}	1.19×10^{-13}	1.91×10^{-13} 2.27×10^{-13}[a]	3.09×10^{-13}	2.10×10^{-13}
	Shear rate constant	2.04×10^{-13} 2.40×10^{-13}[a]	3.14×10^{-13}	2.02×10^{-13}	1.07×10^{-13} 7.38×10^{-14}[a]	7.14×10^{-14}	1.26×10^{-13}
$\frac{15}{15}$	Shear stress constant	1.20×10^{-13} 1.16×10^{-13}[a]	8.59×10^{-14}	1.24×10^{-13}	–	–	–
	Shear rate constant	2.40×10^{-13} 2.84×10^{-13}[a]	3.14×10^{-13}	2.44×10^{-13}	–	–	–
$\frac{23}{7}$	Shear stress constant	1.11×10^{-13} 1.04×10^{-13}[a]	8.59×10^{-14}	1.31×10^{-13}	–	–	–
	Shear rate constant	2.89×10^{-13} 3.09×10^{-13}[a]	3.14×10^{-13}	3.09×10^{-13}	–	–	–

[a] Results obtained by using the experiment data of binary blend.

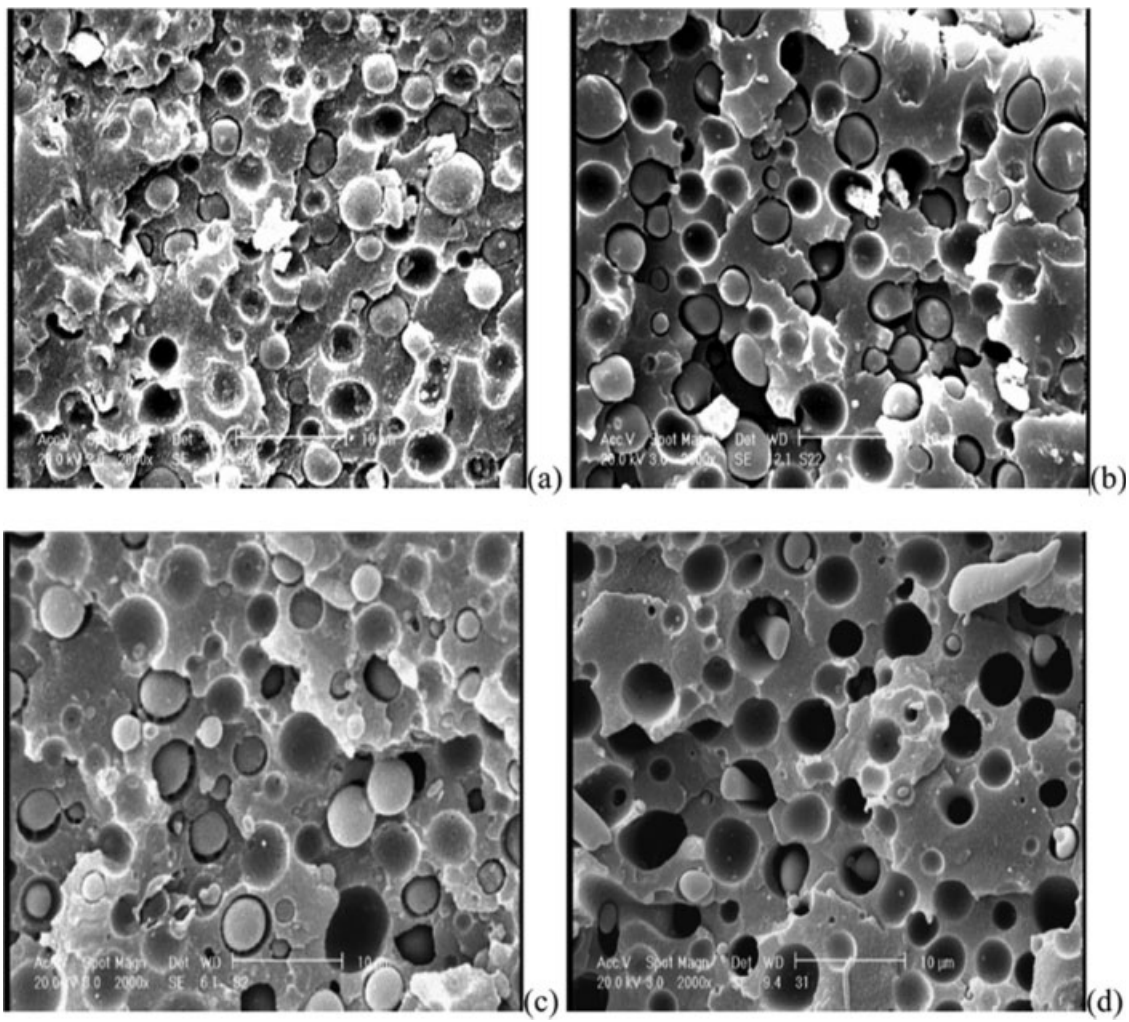

Figure 4 Morphology of PET/H-EVA/PP ternary blend after toluene etching: (a) (70/5/25); (b) (70/10/20); (c) (70/15/15); (d) (70/23/7).

This phenomenon was not observed in PET/PP or PET/EVA binary blends. Figure 7 shows morphology of three binary blends, PET/PP(90/10), PET/H-EVA (90/10) and PET/L-EVA(90/10). Mechanical properties of the mentioned blends will be investigated in another article.

Figure 8(a) shows the volume average diameter D_v of the core-shell dispersed phase versus EVA content at a fixed dispersed phase content of 30%. For H-EVA containing blends, as the quantity of H-EVA is increased from 0 to 100% (based on the dispersed phase volume content), the diagram can be divided to three regions: (i). Sudden reduction of particle size in low content of H-EVA, (ii). Increase of particle size in mean content of H-EVA and (iii). Gradual increase of particle size in high content of H-EVA. The first two regions observed by Reignier et al.[16] but the third one was not seen by them. With increasing the amount of H-EVA the core shell particle size decreased from 5.18 to 1.9 μm and then increased up to 6.5 μm. On the other hand for the droplets with L-EVA shell, when the quantity of L-EVA is increased from 0 to 33%, D_v increased from 5.18 to 7 μm and then decreased to 5.6 μm; and with more increase in L-EVA content we got to cocontinues morphology. Now this is the question: How can we interpret this observation? A similar procedure -just as the ternary blends containing H-EVA in this article was observed by Favis and Reignier[16] for HDPE/PS/PMMA ternary blends. Their logic for this system says: for the blends containing H-EVA, with increasing the amount of H-EVA up to 33%, because of emulsification affects the droplet size decreases and the shell phase thoroughly covers the core, above the 33% the emulsification effects disappear and because of the increment in the droplet to matrix viscosity ratio, the droplet size increases. To complete Reignier's opinion, it seems necessary to declare that the subsequent rise up in D_v [region (iii) in Fig. 8(a)] would correspond to the increment of the droplet to matrix elasticity ratio as an important factor which can influence the droplet size (see Table

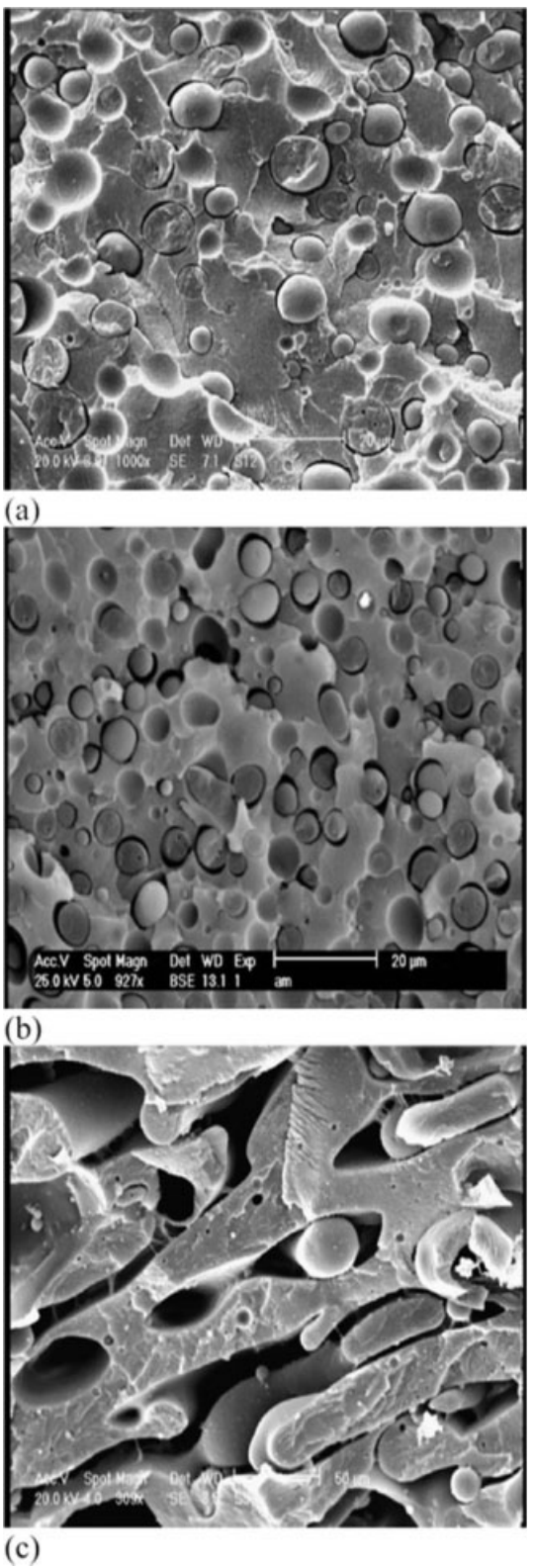

Figure 5 Morphology of PET/L-EVA/PP ternary blend after etching: (a) (70/5/25); (b) (70/10/20); (c) (70/15/15).

I for N_1 values of each phase). Regnier[32] reported that in HDPE/PS/PMMA (with HDPE as a matrix) system, with increasing PS amount up to 60% (based on disperse phase volume content) the droplet diameter increases and after that becomes constant. At this composition, the droplet size is equal to PS droplet size in PS/HDPE (shell/matrix) binary blends. He acclaimed that this behavior is related to the interfacial slip. In the present ternary system, in contrast to the system studied by Reignier et al.[16] elasticity of shell is higher than core, therefore average elasticity of core-shell droplets increases with increase of shell thickness. It is worth noting that when the composition of the shell based on disperse phase exceeds 60% the effect of droplet average viscosity increment on increasing of the core-shell droplet size weakens; as already mentioned by Reignier et al.[16] The droplet size increase after that critical composition is because of the increase in the average droplet elasticity compared to the matrix elasticity, it is necessary to declare that Reignier didn't investigate the elasticity effect. According to Vanoene's[25] equation for the droplets with more elasticity than that of the matrix phase, by increasing the droplet elasticity, the interfacial tension increases and this leads to the increase of the droplet size. Van oene's[25] equation is as below:

$$\gamma_{dm} = \gamma^0_{dm} + \frac{R_d}{6}(N_{1,d} - N_{1,m}) \tag{16}$$

where γ_{dm} is the dynamic interfacial tension of droplet (d) in matrix (m); γ^0_{dm}, the interfacial tension in the absence of flow; R_d, the droplet diameter; $N_{1,d}$ and $N_{1,m}$ are the first normal stress functions of the dispersed and matrix phase respectively.

For the ternary blends containing L-EVA as the shell, the droplet behavior is more complex. Figure 8(a) shows that with increasing 5% L-EVA to the PET/PP binary system, the droplet size increased but more amounts caused it to decrease. When L-EVA amount increases from 5 to 10%, the droplet size decreased, that is related to the average droplet viscosity decrement in this condition. Increasing the droplet size from PET/PP(70/30) binary blend to PET/L-EVA/PP(70/5/25), could be attributed to the coalescence effect, when L-EVA is the shell phase, coalescence increases. Reignier et al.[14] showed that in HDPE/PS/PMMA system (with HDPE as a matrix) composite droplets experience a dual coalescence process, first between PMMA subinclusions within composite droplets, and second between composite droplet themselves. According to the calculation of diameter of PP core phase in PET/L-EVA/PP(70/5/25) ternary blends, it is concluded that the size of PP core in ternary blends is higher than its size in PET/PP(70/25) binary blends. At a glance, it seems that this is due to the presence of shell particles in PP core, but it is evident that they are less than required volume for observed diameter

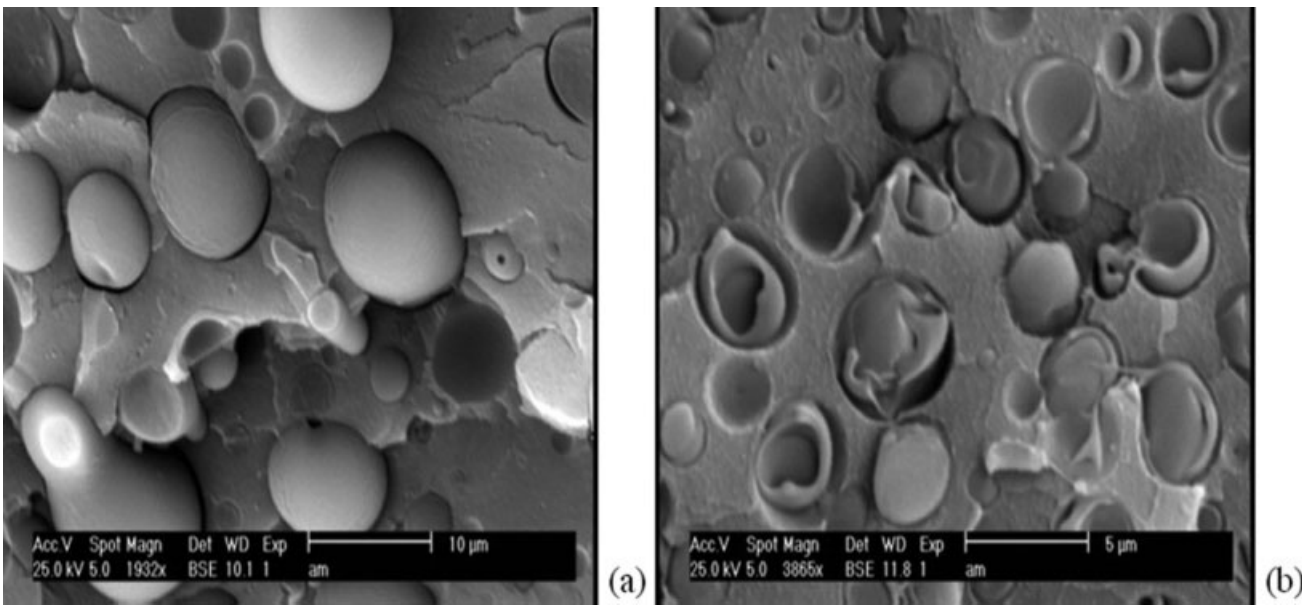

Figure 6 (a) Binary blends of PET/H-EVA(70/30) without etching (b) Ternary blends of PET/H-EVA/PP(70/15/15) without etching.

increment. Therefore, it conjectures that because of low molecular weight of L-EVA coalescence between composite droplets easier occurred and after that PP cores coalescences.

For better understanding of increasing coalescence with presence of L-EVA, Coalescence effects under dynamic mixing conditions are examined by observing the dispersed particle size/composition relationship. At low concentrations of dispersed phase, when the blend is fine dispersed, the average droplet diameter is the consequent of the dynamic equilibrium in the division and coalescence phenomena controlling the size of the droplets in the blend. It has been shown that a low interfacial tension PVC/LLDPE blend revealed almost no change in particle size with composition.[33] This blend then does not experience significant dynamic coalescence phenomena during melt mixing. In the same way, the existence of an interfacial agent in a binary blend leads to a reduction of the particle size with composition, again due to the avoidance of coalescence through immobilization of interface and reduction of the interfacial tension.[34]

Figure 8(b) shows that particle size of PET/L-EVA/PP(90/5/5) ternary blend is between particle sizes of PET/PP and PET/L-EVA binary blends. In comparison with PET/PP binary blends it can be concluded that L-EVA causes to more compatibility between PP and PET, and consequently decreases the particle size of ternary blends. Average viscosity of core-shell particle is also higher than L-EVA and less than PP droplets. Therefore it is logic that the particle size of PET/L-EVA/PP(90/5/5) ternary blend is between PET/PP(90/10) and PET/L-EVA(90/10) binary blends. Interesting results are obtained with increasing of disperse phase content. Cocontinuous morphology is obtained in PET/L-EVA(80/20) blends. It is interesting that core-shell particle size of PET/L-EVA/PP(80/10/10) is larger than particle size of PET/PP(80/20) blend. Although L-EVA, as a compatibilizer, should decrease the rate of particle size increment with disperse phase concentration. Because of low molecular weight of L-EVA increment of disperse phase content intensify the effect of coalescence that it is a proof of our previous discussion. Deep investigation of composition effects on the morphology and rheology of ternary polymer blends is subject of our future work.

The results reported in this work indicate that for the blends and viscosity ratios studied here, the core–shell morphology encountered is the one thermodynamically predicted by the spreading coefficient model and independent of the viscosity ratio of both dispersed phase. When using H-EVA, the component with higher viscosity encapsulates the component with lower viscosity. The type of morphology did not change even when the composition of the minor phases changed from 5/25 to 23/7. As a conclusion, unlike the theory reported by some authors,[18,19] we claim that the viscosity ratio of the two minor phases does not exert an influence to the formation of the core–shell morphology.

According to Figure 9 two points should be considered. First; in the ternary blends containing L-EVA, even with a 5% content of L-EVA the shell phase thoroughly covers the core, unlike the systems containing H-EVA. It can be related to L-EVA lower molecular weight. Second, the phenomenon of

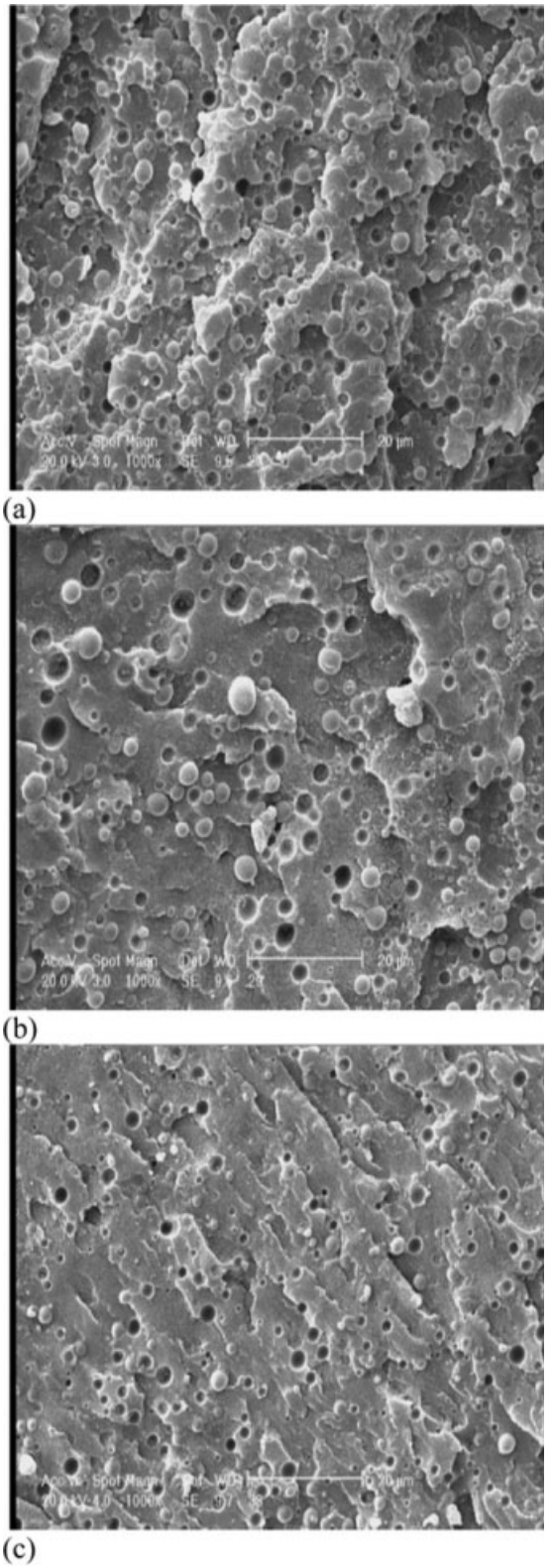

Figure 7 Micrographs of binary blends of (a) PET/PP(90/10), (b) PET/H-EVA(90/10) (c) PET/L-EVA(90/10).

subinclusion of the shell within the core occurred in the case of blends containing L-EVA and not for those of H-EVA even for all ranges of H-EVA content. Lusinov et al.[20] reported that the subincusion of the shell into the core represents the tendency of core to engulf the shell phase for the core contents larger than theoretical that of phase inversion in related core shell binary blend. They used the following equation to predict the phase inversion of binary blends:

$$\frac{\eta_1}{\eta_2} = \frac{\Phi_1}{\Phi_2} \tag{17}$$

where η_1 and η_2 are the viscosity of polymeric melts at constant shear rate, and Φ_1 and Φ_2 are the volume fraction of polymers 1 and 2, respectively.

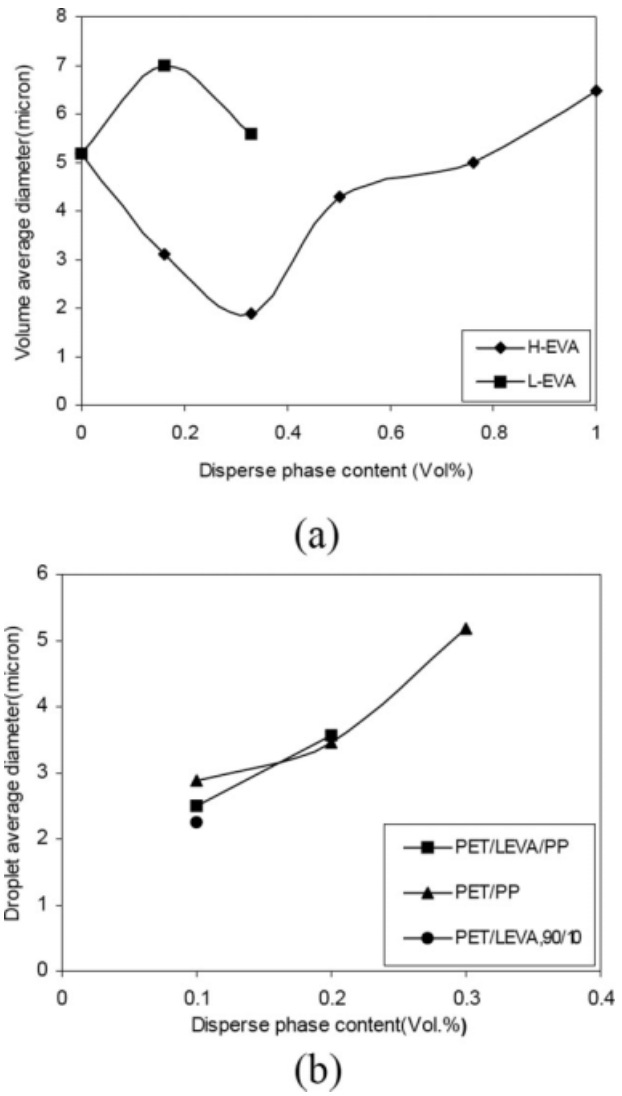

Figure 8 (a) Disperse phase diameter as a function of EVA content in the disperse phase for the 70(PET)/30(EVA+PP); (b) Dispersed phase diameter as a function of the dispersed phase content for PET/L-EVA/PP ternary blends where L-EVA/PP = 1. Comparison with PET/PP and PET/L-EVA binary blends. In all cases PET is the matrix.

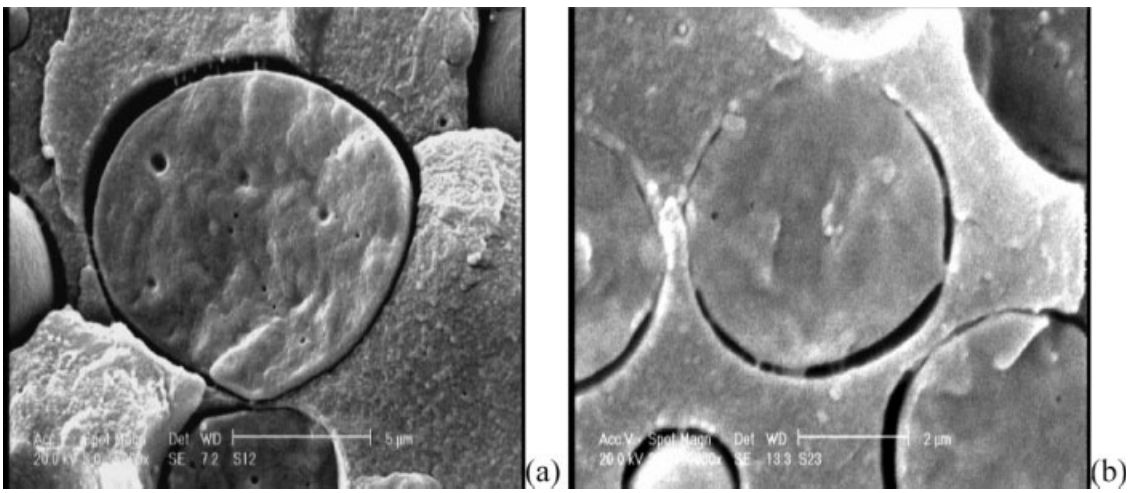

Figure 9 SEM micrographs of the: (a) PET/L-EVA/PP(70/5/25); (b) PET/H-EVA/PP(70/5/25).

Reignier et al.[16] reported that, during the initial stage of mixing, the shell could be immobilized by the core because it has a higher viscosity. This event leads to segregation in the core-shell structure. They changed the core viscosity and observed subinclusion of shell within the core with higher viscosity. But, in this research work, shell viscosity was changed and subinclusion of the shell with lower viscosities was observed. The two evidences mentioned above, are compared here; but for this system, initial stage of mixing is contradictory with Reignier's work. Using equation 17 and viscosity values of molten polymers in shear rate of 150 s^{-1}, the PP contents in which the phase inversion occurs were predicted 23 and 90% for PP/H-EVA and PP/L-EVA binary blends, respectively. On the basis of dispersed phase, the PP concentration in the PET/H-EVA/PP(70/5/25) blend is 83% (% vol) which is above the phase inversion concentration in the related H-EVA/PP(5/25) binary blend. According to Luzinov, EVA subinclution should be observed, whereas it is not observed in present system. On contrary in the PET/L-EVA/PP(70/5/25) system, if core shell droplets observed as matrix disperse, L-EVA is the matrix phase for PP/L-EVA binary blend. This phenomenon was also predicted by equation 17 so PP does not tended to be shell phase but subinclusions of shell in the core phase were observed. According to previous discussion, it can be concluded that tangling of small particles of L-EVA is the main reason of subinclusion formation rather than thermodynamic tendency in PP viscose phase.

Figure 10 shows multi core-shell structure in PET/H-EVA/PP (70/23/7) ternary blend. Some authors observed that with increasing the shell thickness, core–shell morphology changes to multi core-shell. Luzinov et al.[27] introduced the term "multi core structure" to describe the case where several subinclusions of one minor phase are trapped in large particle of the second minor phase. Reignier et al.[16] studied HDPE/PS/PMMA systems with two types of high viscosity and low viscosity PMMA (H-PMMA and L-PMMA). They observed that in the L-PMMA containing systems core–shell morphology forms at significantly lower PMMA compositions than that of H-PMMA which forms multicore structure. For explanation of this phenomenon we assume core-shell droplets as matrix disperse, the shell phase is assumed to be matrix and the core is assumed to be the dispersed phase. It is obvious that with increasing the amount of disperse phase, coalescence increases; with higher amounts of core forming polymer, we get to core–shell morphology.

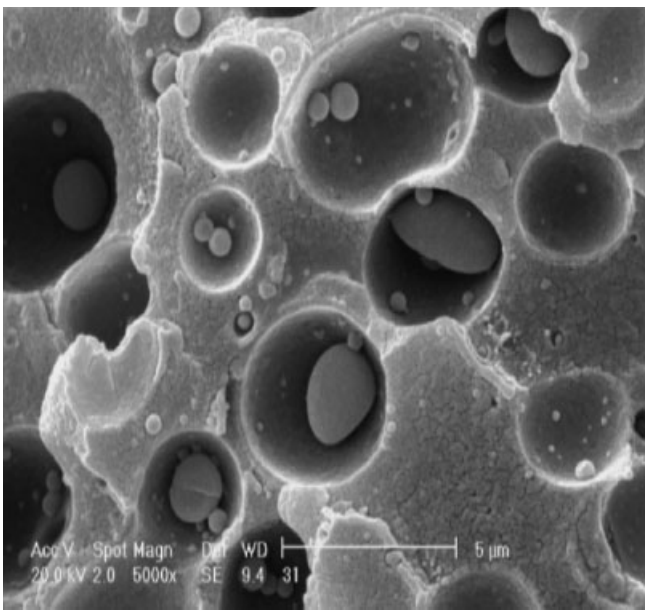

Figure 10 Multi core structure in PET/H-EVA/PP, 70/23/7.

When the amount of dispersed phase (core phase) decreases, coalescence decreases too.

CONCLUSIONS

In this work, the morphologies of PET/H-EVA/PP and PET/L-EVA/PP ternary blends were studied. In both systems, core-shell morphologies in which PP had been encapsulated by EVA were observed. Models based on the interfacial free energy and the spreading coefficient; predict the same morphology for each ternary system as the microscopy results. The dynamic interfacial energy model was applicable for the systems containing H-EVA and L-EVA in constant shear stress state and constant shear rate method, respectively. It seems that stress at the L-EVA/PP interface is not equal to matrix average stress. Therefore, for system containing L-EVA, estimation of N_1 value at the matrix stress is not true.

In ternary blends containing H-EVA and L-EVA, it was observed that the changes in droplet size with core/shell ratio are completely different from each other. Droplets with L-EVA shell, introduce an unusual larger size rather than droplets with H-EVA shell, which would be attributed to the lower molecular weight of L-EVA. It suggests that L-EVA intensify the coalescence effect. This phenomenon was also proved by changing the disperse phase content of ternary blends and comparison with related binary blends. It was shown that the increase of L-EVA causes an increment and then a decrement in the droplet size, while increasing the concentration of H-EVA in blends with the constant disperse phase, first decreased and then increased the core-shell particle size.

When L-EVA is the shell phase, subinclusion of L-EVA into the core was observed; but for the blends containing H-EVA as the shell, this microstructure wasn't observed. This observable fact is related to trapping during mixing process. In the samples containing H-EVA, core–shell morphology changed to multi core structure with H-EVA content.

References

1. Robeson, L. M. Polym Eng Sci 1984, 24, 587.
2. Xanthos, M. Polym Eng Sci 1988, 28, 1392.
3. Utracki, L. A. Polym Networks Blends 1991, 1, 61.
4. Favis, B. D.; Chalifoux, J. P. Polymer 1988, 29, 1761.
5. Favis, B. D. J Appl Polym Sci 1990, 39, 283.
6. Favis, B. D.; Chalifoux, J. P. Polym Eng Sci 1987, 27, 1591.
7. Willis, J. M.; Favis, B. D. Polym Sci 1990, 28, 2259.
8. Wu, S. Polym Eng Sci 1987, 27, 335.
9. Nauman, E. B.; He, D. Q. Chem Eng Sci 1999, 2001, 56.
10. Urashita, S.; Kawakatsu, T.; Doi, M. Prog Theor Phys Suppl 2000, 138, 412.
11. Horiuchi, S.; Matchariyakul, Y. K.; Kitano, T. Macromolecules 1997, 30, 3664.
12. Guo, H. F.; Packirisamy, S.; Gvozdic, N. V.; Meier, D. J. Polymer 1997, 38, 785.
13. Guo, H. F.; Gvozdic, N. V.; Meier, D. J. Polymer 1997, 38, 4915.
14. Reignier, J.; Favis, B. D. Macromolecules 2000, 33, 6998.
15. Reignier, J.; Favis, B. D.; Heuzey, M. C. Polymer 2003, 44, 49.
16. Reignier, J.; Favis, B. D. AIChE J 2003, 49, 1014.
17. Hobbs, S. Y.; Dekkers, M. E. J.; Watkins, V. H. Polymer 1998, 29, 1598.
18. Nemirovski, N.; Siegmann, A.; Narkis, M. J. Macromol Sci Phys 1995, B34, 459.
19. Gupta, A. K.; Srinivasan, K. R. J Appl Polym Sci 1993, 47, 167.
20. Lusinov, I.; Pagnoulle, C.; Jérôme, R. Polymer 2000, 41, 7099.
21. Hemmati, M.; Nazokdast, H.; Panahi, H. S. J Appl Polym Sci 2001, 82, 1129.
22. Valera, T. S.; Morita, A. T.; Demarquette, N. R. Macromolecules 2006, 39, 2663.
23. Legros, A.; Carreau, P. J.; Favis, B. D.; Michel, A. Polymer 1997, 38, 5085.
24. Harkins, W. D. The Physical Chemistry of Surface Films; Reinhold: New York, 1952; p 23.
25. Van Oene, H. J Colloid Interface Sci 1972, 40, 448.
26. Kim, B. K.; Kim, M. S.; Kim, K. K. J Appl Polym Sci 1993, 48, 1271.
27. Luzinov, I.; Xi, K.; Pagnoulle, C.; Huynh-Ba, G.; Jérôme, R. Polymer 1999, 40, 2111.
28. Bousmina, M.; Ait-Kadi, A.; Faisant, J. B. J Rheol 1999, 43, 415.
29. Wu, S. In Polymer Handbook, 4th ed.; Brandrup, J., Immergut, E. H., Grulke, E. A., Eds.; Wiley: New York, 1999.
30. Cox, W. P.; Merz, E. H. J Polym Sci 1958, 28, 619.
31. Laun, H. M. J Rheol 1986, 30, 459.
32. Leclair, A.; Favis, B. D. Polymer 1996, 37, 4723.
33. Reignier, J.; Favis, B. D. Polymer 2003, 44, 5061.
34. Liang, H.; Favis, B. D. Macromolecules 1999, 32, 1637.